Real-time Non-visual Shape Estimation and Robotic Dual-Arm Manipulation Control of an Elastic Wire

Itamar Mishani and Avishai Sintov

***Abstract*—The dual-arm manipulation of elastic wires has been a hard problem for many decades. Nevertheless, recent work has shown that the shape of a wire can be defined by a very simple representation. Theoretical analysis has stated that simple sensing of the force and torque at one end of the wire can be used to determine its shape. In this letter, we experimentally analyze the developed theoretical foundation. We deploy a dual-arm robotic system able to accurately manipulate an elastic wire. The system does not require complex visual perception and is able to reason about the shape of the wire by solely sensing forces and torques on one arm. Furthermore, we propose a full framework in which the mechanical properties of the wire are rapidly approximated in real-time. Then, a simple control rule based on Force/Torque feedback is used to manipulate the wire to some goal or track a planned path. We conduct various experiments on a full-scale system to analyze pose estimation and control accuracies. Results validate the benefit of the approach and demonstrate the ability to accurately manipulate a wire.**

***Index Terms*—Elastic wires, Dual Arm Manipulation, Manipulation Planning.**

I. Introduction

THE manipulation of thin elastic wires has been of interest for centuries [1]. Wire manipulation is considered a difficult task to operate in industrial environments. The common approach to manipulate deformable objects is using two robotic arms [2], [3]. However, in order to efficiently and safely manipulate wires, one requires sufficiently accurate models and control schemes. Once achieved, wire manipulation abilities for robots would be practical in many applications. For instance, cable routing is still operated manually in automotive production lines [4]. Other applications include knot tying [5], surgical suturing [6], hot wire carving recently demonstrated by a robotic system [7] or manipulation of cables using autonomous aerial vehicles [8].

The configuration space describing the shape of an elastic wire has infinite dimension. Moreover, a multitude of wire shapes exists for a single pose of the robot arms holding it by the tips. These challenges have made the manipulation planning of a wire a challenging problem. Prior work on path planning for elastic wires suggest exploring the set of equilibrium configurations indirectly, by sampling displacements of grippers and using numerical simulations to approximate their effect on the wire [9], [10]. Hermansson et al. [11] relaxed handle constraints along an elastic harness and planned a collision-free path for a central grip point. These approaches use computationally expensive simulation-based methods that may limit their effectiveness in real-time motion planning. Another approach simplified the model of a deformed object by reducing it to a sequence of rigid masses and springs [12]. Similarly, a soft robot was discretized in order to compute a collision-free path in a confined space [13]. In these approaches, the solutions use coarse discretization which do not scale to high-dimensional cases and, in turn, affect the quality of the planning. A feasible procedure to derive the free configuration space of an elastic wire was not yet clear at the time. Seminal work by Bretl and McCarthy [14] later showed that the configuration space of the wire, i.e., the set of all equilibrium configurations, is a six-dimensional smooth manifold. Such revelation enabled the use of sampling-based planning algorithms to plan stable and collision-free paths [15], [16].

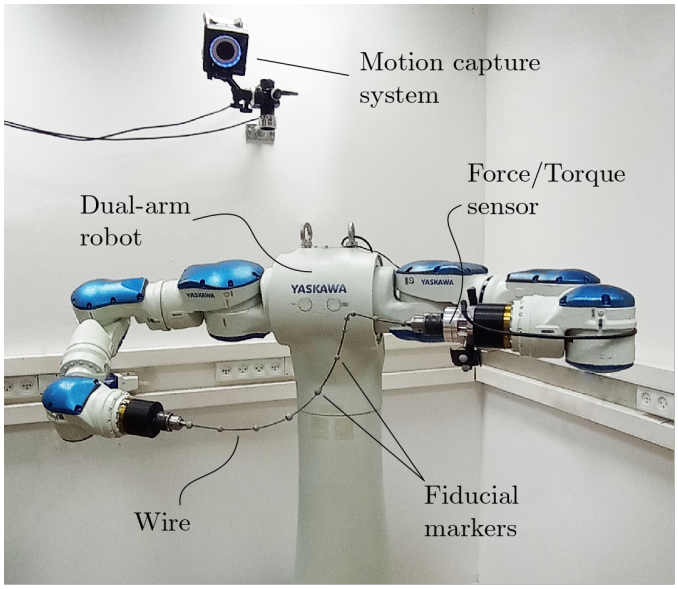

Fig. 1. A dual-arm robot manipulating an elastic wire. The shape of the wire is estimated solely using Force/Torque sensing on one gripper.

Many attempts have been made to estimate and control the shape of an elastic wire. Borum et al. [17] used fiducial markers and images to approximate the shape of a planar wire. The work in [18] demonstrated the estimation of a thin elastic strip using a force sensor and based on a discretized Kirchhoff elastic rod model. In [19], a simulated discrete elastic rod model is fitted on data obtained from camera images. In [20], a cable is parameterized by a Fourier series while the parameters are estimated using image segmentation. Using the model, velocity control is utilized to deform the cable into desired

Manuscript received: September 9, 2021; Accepted: November, 08, 2021.
This paper was recommended for publication by Editor Eric Marchand upon evaluation of the Associate Editor and Reviewers' comments.
I. Mishani and A. Sintov are with the School of Mechanical Engineering, Tel-Aviv University, Israel. e-mail: {mishani1, sintov1}@{mail,tauex}.tau.ac.il.
Digital Object Identifier (DOI): .

shapes. However, visual perception and image segmenting of thin objects such as a wire in a cluttered environment is a challenging task. Moreover, relying on continuous visual feedback limits the performance of various tasks in which visual uncertainty (e.g., poor lighting or shadows) or occlusion may occur. This may include manipulating the wire within a confined space such as a vehicle frame. The work of Takano et al. [21] uses a Force/Torque sensor to estimate the shape of a thin strip based on a discrete model. Mechanical properties are not estimated and assumed to be known. While reducing the problem to a finite-dimensional space, these approaches are highly dependent on the resolution of the discretization and directly proportional to computation time. In addition, these methods focus mostly on shape estimation and do not provide an efficient ability to plan and control wire motions.

In this letter, we propose a full framework to identify, plan and control the motion of an elastic wire using a dual-arm robot without visual perception. Theoretical analysis in [14] has shown that the configuration of a wire is, in fact, the force and torque exerted at one end of the wire. Hence, we utilize a Force/Torque (F/T) sensor to measure the load exerted on one gripper by the wire (Figure 1). We explore the sole use of the load measurement to accurately estimate the shape of wire. Our framework first estimates the mechanical parameters of the wire in real-time based only on F/T measurements and gripper poses. The accuracy of the shape estimation based only on load sensing is then analyzed over various wires. Furthermore, we propose a simple and novel control scheme to reach a desired configuration and track a planned path. Inaccurate tracking of a planned path may lead to wire instability and collision with obstacles. During a collision, the model deviates from the basic assumptions of the model (i.e., two fixture points) and predictions are not possible. Hence, accurate tracking of a path in a confined space is essential. To the best of the author's knowledge, this is the first implementation and experimental analysis of the theoretical foundation developed by Bretl and McCarthy [14] for shape estimation of spatial elastic wires using F/T measurements with a full scale dual-arm robotic system.

II. Background

In this section, we briefly present the theoretical background from Bretl and McCarthy [14]. Their work showed that each equilibrium configuration of a Kirchhoff elastic rod [22] corresponds to a unique point in a subset of $\mathbb{R}^6$. Furthermore, it was shown that a configuration is, in fact, the force and torque exerted at the base of the wire.

A. The configuration space of an elastic wire

We assume a wire of length L that is straight in the undeformed configuration with high enough stiffness so that the effects of gravity can be neglected. Using $t \in [0, L]$ to denote arc-length along the wire, the position and orientation of the wire at arc-length t are described by an element $\mathbf{q}(t)$ of the special Euclidean group $SE(3)$. The wire's shape is described by a continuous map $\mathbf{q}\colon [0, L] \to SE(3)$. In the Kirchhoff model, the wire is allowed to twist and bend, but is unshearable and inextensible [22]. These constraints are enforced by requiring q to satisfy the differential equation

$$\dot{\mathbf{q}} = \mathbf{q} \begin{pmatrix} \widehat{\mathbf{u}} & e_1 \\ 0 & 0 \end{pmatrix}, \tag{1}$$

for some function $\mathbf{u}\colon [0, L] \to \mathbb{R}^3$, where overdots denote differentiation with respect to t, the map $\widehat{\ }\colon \mathbb{R}^3 \to \mathfrak{so}(3)$ satisfies $a \times b = \widehat{a}b$ for all $a, b \in \mathbb{R}^3$, and $e_1 = [1\ 0\ 0]^T$.

We assume that each end of the wire is held by a robotic gripper. The position and orientation of each point $q(t)$ on the wire is represented relative to the gripper at $t = 0$ (referred to as the *base gripper*) such that $q(0) = I$, where $I \in SE(3)$ is the identity matrix. This establishes the initial condition for differential equation (1). Furthermore, let $\mathcal{B} \subset SE(3)$ denote the space of boundary conditions at $\mathbf{q}(L)$, the configuration of the gripper holding the wire at $t = L$ (referred to as the *second gripper*) is denoted by $\mathbf{b} \in \mathcal{B}$.

We define the set $\mathcal{A} \subset \mathbb{R}^6$ by

$$\mathcal{A} = \{\mathbf{a} \in \mathbb{R}^6 : (a_2, a_3, a_5, a_6) \neq (0, 0, 0, 0)\} \tag{2}$$

The set $\mathcal{A}$ is simply $\mathbb{R}^6$ with a two-dimensional plane removed. Each point in $\mathcal{A}$ corresponds to an equilibrium configuration of the wire and a local minimum of the total elastic energy of the wire. Proof for this can be viewed in Theorem 5 of Bretl and McCarthy [14]. Thus, one can solve the following six ordinary differential equations

$$\begin{aligned} \frac{d\mu_1}{dt} &= \frac{\mu_3\mu_2}{c_3} - \frac{\mu_2\mu_3}{c_2} & \frac{d\mu_4}{dt} &= \frac{\mu_3\mu_5}{c_3} - \frac{\mu_2\mu_6}{c_2} \\ \frac{d\mu_2}{dt} &= \mu_6 + \frac{\mu_1\mu_3}{c_1} - \frac{\mu_3\mu_1}{c_3} & \frac{d\mu_5}{dt} &= \frac{\mu_1\mu_6}{c_1} - \frac{\mu_3\mu_4}{c_3} \\ \frac{d\mu_3}{dt} &= -\mu_5 + \frac{\mu_2\mu_1}{c_2} - \frac{\mu_1\mu_2}{c_1} & \frac{d\mu_6}{dt} &= \frac{\mu_2\mu_4}{c_2} - \frac{\mu_1\mu_5}{c_1} \end{aligned} \tag{3}$$

on the interval $t \in [0, L]$ with the initial condition $\mu(0) = \mathbf{a}$ for $\mathbf{a} \in \mathcal{A}$. In addition, $c_1 > 0$ is the torsional stiffness of the wire and $c_2, c_3 > 0$ are the bending stiffnesses. Next, functions $u_1\colon [0, L] \to \mathbb{R}$ and $u_2, u_3\colon [0, L] \to \mathbb{R}$ are the twisting and bending strains along the wire, respectively, such that $\mathbf{u} = (u_1, u_2, u_3)^T$ and $u_i = \mu_i / c_i$ for $i = 1, 2, 3$. Solving (1) with the resulting $\mathbf{u}$ produces an equilibrium shape of the wire, denoted by the pair of functions $(\mathbf{q}, \mathbf{u})$. Each $(\mathbf{q}, \mathbf{u})$ and the corresponding μ are completely defined by the choice of $\mathbf{a} \in \mathcal{A}$. Therefore and in practice, $\mathcal{A}$ serves as the configuration space of the wire. The resulting map is defined by $\mathcal{C} = \Phi(\mathcal{A})$. The map Φ is injective, i.e. for each $(\mathbf{q}, \mathbf{u}) \in \mathcal{C}$ there exists a unique $\mathbf{a} \in \mathcal{A}$ such that $(\mathbf{q}, \mathbf{u}) = \Phi(\mathbf{a})$. Furthermore, one may solve for matrix $\mathbf{J} : [0, L] \to \mathbb{R}^{6\times 6}$, the following linear arc-length-varying matrix differential equations

$$\dot{\mathbf{M}} = \mathbf{F}(\mu(t))\mathbf{M} \qquad \dot{\mathbf{J}} = \mathbf{G}\mathbf{M} + \mathbf{H}(\mu(t))\mathbf{J} \tag{4}$$

with initial conditions $\mathbf{M}(0) = I$ and $\mathbf{J}(0) = 0$. Definitions for $\mathbf{G}$, $\mathbf{F}(\cdot)$ and $\mathbf{H}(\cdot)$ are given in [14]. Here also, the matrices $\mathbf{M}$ and $\mathbf{J}$ are completely defined by the choice of $\mathbf{a} \in \mathcal{A}$.

We denote the set of all $\mathbf{a} \in \mathcal{A}$ that correspond to stable equilibrium configurations by $\mathcal{A}_{stable}$. A configuration $(\mathbf{q}, \mathbf{u})$ is a stable equilibrium configuration if $\det(\mathbf{J}(t)) \neq 0$ for all $t \in (0, L]$. Hence, we have a numerical test for each configuration $\mathbf{a} \in \mathcal{A}$ to determine which equilibrium configurations of the wire is in $\mathcal{A}_{stable}$. We define the free configuration space

$\mathcal{A}_{free} \subset \mathcal{A}_{stable}$ to be the set of all $\mathbf{a} \in \mathcal{A}$ that correspond to stable equilibrium configurations of the wire and do not contain self-intersections. We next define the map $\Psi : \mathcal{C} \to \mathcal{B}$ such that a configuration $(\mathbf{q}, \mathbf{u})$ is mapped to $\mathbf{q}(L)$. Given a path of the wire in $\mathcal{C}_{stable}$, the function Φ can be used to find the path of the robotic gripper that causes the wire to follow the path in $\mathcal{C}_{stable}$. In particular, the map

$$\Gamma : \mathcal{A}_{stable} \to \mathcal{B}_{stable}, \tag{5}$$

where $\Gamma = \Phi \circ \Psi$, takes $\mathbf{a} \in \mathcal{A}_{stable}$ to the corresponding pose of the second gripper $\mathbf{b} = \mathbf{q}(L) \in \mathcal{B}_{stable}$. Map Γ is a *local diffeomorphism* [14].

B. Physical meaning of $\mathbf{a} \in \mathcal{A}$

The resulting function $\boldsymbol{\mu}\colon [0, L] \to \mathbb{R}^6$ can be interpreted as the vector of internal forces and torques along the wire. Therefore, we can describe the force and torque at point t along the wire as

$$\mathbf{f}(t) = (\mu_4(t), \mu_5(t), \mu_6(t))^T \tag{6}$$

$$\boldsymbol{\tau}(t) = (\mu_1(t), \mu_2(t), \mu_3(t))^T, \tag{7}$$

respectively, where $\mu_j(t)$ is the j^{th} component of $\boldsymbol{\mu}(t)$ [14]. Consequently and since Φ is injective, any equilibrium configuration $\mathbf{a} = \boldsymbol{\mu}(0)$ is completely defined by the force $\mathbf{f}(0)$ and torque $\boldsymbol{\tau}(0)$ at the base gripper. In other words, by solely measuring the load exerted on the gripper using a F/T sensor, one can directly acquire the configuration $\mathbf{a}$ and, using $\Phi(\mathbf{a})$, solve for the shape of the wire $\mathbf{q}$. Similarly, the load measurement provides the expected position of the second gripper $\mathbf{b}$.

III. METHOD

Given two robotic arms with a Force/Torque (F/T) sensor mounted on one arm. The arms hold a wire of length L and mechanical coefficients $\mathbf{c} = (c_1, c_2, c_3)^T$ by its end-tips. We aim to use the measurement $\tilde{\mathbf{a}} \in \mathcal{A}$ of the F/T sensor to approximate the shape of the wire $\tilde{\mathbf{q}}$. Motion of the wire is considered to be quasi-static in order to maintain equilibrium configurations. In this section, we present the proposed framework accurately manipulate a given wire. A scheme of the framework is illustrated in Figure 2. We first describe the process to estimate the length and coefficients of a new wire solely using F/T measurements and second gripper pose $\mathbf{b}$. Then, we propose an easy to implement rule to control the shape of the wire.

A. Perturbation mapping from $\mathcal{A}$ *to* $\mathcal{B}$

Given $\mathbf{a}_i \in \mathcal{A}_{stable}$ and its corresponding end-tip pose $\mathbf{b}_i = \Gamma(\mathbf{a}_i)$. We define an homogeneous transformation matrix $M \in SE(3)$ with $\delta\mathbf{x} \in \mathbb{R}^3$ and exponential coordinates $\mathbf{w} \in \mathbb{R}^3$ and $\delta\theta \in [0, \pi)$ such that

$$M(\delta\mathbf{b}) = \begin{bmatrix} e^{\mathbf{w}\delta\theta} & \delta\mathbf{x} \\ \mathbf{0} & 1 \end{bmatrix}, \tag{8}$$

where

$$\delta\mathbf{b} = \begin{pmatrix} \mathbf{w}\delta\theta \\ \delta\mathbf{x} \end{pmatrix}. \tag{9}$$

Matrix M is defined to map between two configurations in $\mathcal{B}$ such that

$$\mathbf{b}_{i+1} = \mathbf{b}_i M(\delta\mathbf{b}) \tag{10}$$

where perturbation to $\mathbf{b}_{i+1}$ will result in wire configuration $\mathbf{a}_{i+1}$. Map Γ is a local diffeomorphism being smooth and has a non-singular Jacobian matrix $\mathbf{J}(L)$. From Theorem 7 and equation (37) in [14], we get that

$$\delta\mathbf{b} \approx \mathbf{J}(L)\delta\mathbf{a} \tag{11}$$

where $\delta\mathbf{a} = \mathbf{a}_{i+1} - \mathbf{a}_i$. Equation (11) states that matrix $\mathbf{J}(L)$ contains information about the relationship between small changes in $\mathcal{A}$ and small changes in $\mathcal{B}$. Therefore and given a desired $\mathbf{a}_{i+1}$ in the vicinity of $\mathbf{a}_i$, the required perturbation $\delta\mathbf{a}$ in $\mathcal{A}$ can be obtained. Then, by solving (11), one can use map (10) to compute the required perturbation in $\mathcal{B}$ in order to move a wire from configuration $\mathbf{a}_i$ to $\mathbf{a}_{i+1}$.

B. Real-time approximation of $\mathbf{c}$ *and* L

Given a measurement $\tilde{\mathbf{a}}_j$ of the F/T sensor, one can solve $(\mathbf{q}_j, \mathbf{u}_j) = \Phi(\tilde{\mathbf{a}}_j)$ with (3) to acquire the current shape q_j of the wire. In order to solve (3), however, one must first estimate the mechanical coefficients vector $\mathbf{c}$ of the wire. Given a wire picked-up by two robotic arms, the information available includes measurements of $\tilde{\mathbf{a}}$ and $\tilde{\mathbf{b}}$. We aim to rapidly compute an estimation $\tilde{\mathbf{c}}$ of $\mathbf{c}$ and the wire length $\tilde{L}$. We first formulate the cost function to be minimized in order to estimate $\mathbf{c}$. Recall that matrix $\mathbf{J}(L)$ is dependent on the choice of $\mathbf{c}$. Hence, (11) implies that differential measurements of $\mathbf{a}$ and $\mathbf{b}$ are required in order to estimate $\mathbf{c}$ and $\mathbf{L}$. We propose a real-time model identification process based on such notion.

While moving the robot arms, a path $\mathcal{B}_c = \{\tilde{\mathbf{b}}_1, \tilde{\mathbf{b}}_2, \ldots, \tilde{\mathbf{b}}_m\}$ of the second gripper relative to the base one is being recorded along with its corresponding vectors of force and torque $\mathcal{A}_c = \{\tilde{\mathbf{a}}_1, \tilde{\mathbf{a}}_2, \ldots, \tilde{\mathbf{a}}_m\}$ exerted on the base gripper. Sets $\mathcal{A}_c$ and $\mathcal{B}_c$ are then used to compute the differential sets $\mathcal{A}'_c = \{\delta\tilde{\mathbf{a}}_1, \delta\tilde{\mathbf{a}}_2, \ldots, \delta\tilde{\mathbf{a}}_{m-1}\}$ and $\mathcal{B}'_c = \{\delta\tilde{\mathbf{b}}_1, \delta\tilde{\mathbf{b}}_2, \ldots, \delta\tilde{\mathbf{b}}_{m-1}\}$, respectively, where $\delta\tilde{\mathbf{a}}_i = \tilde{\mathbf{a}}_{i+1} - \tilde{\mathbf{a}}_i$ and $\delta\tilde{\mathbf{b}}_i$ is computed according to (9)-(10). Also, let $\boldsymbol{\eta} = (\mathbf{c}, L)^T \in \mathbb{R}^4$ be the vector of unknown parameters. Furthermore, we define matrix $\bar{\mathbf{J}}_\eta(\mathbf{a})$ to be the Jacobian $\mathbf{J}(L)$ of configuration $\mathbf{a}$ and computed with η. An approximation of η is the solution of the following problem

$$\begin{aligned} \boldsymbol{\eta}^* = arg\min_{\boldsymbol{\eta}} \quad & \sum_{i=1}^{m-1} \|\bar{\mathbf{J}}_\eta(\tilde{\mathbf{a}}_i)\delta\tilde{\mathbf{a}}_i - \delta\tilde{\mathbf{b}}_i\|^2 \\ \text{s.t.} \quad & \boldsymbol{\eta} > 0. \end{aligned} \tag{12}$$

Problem (12) is non-linear and non-convex with regards to $\boldsymbol{\eta}$ and, therefore, requires a global minimization algorithm. We employ a wire model identification process based on the Particle Swarm Optimization (PSO) [23] algorithm. PSO is a meta-heuristic global optimization algorithm that minimizes some cost function by iteratively improving candidate solutions. The algorithm maintains a population of particles in the search space, i.e., candidate solutions, each having its own cost value. Their position is iteratively updated according to simple mathematical rules. The rules consider the momentary

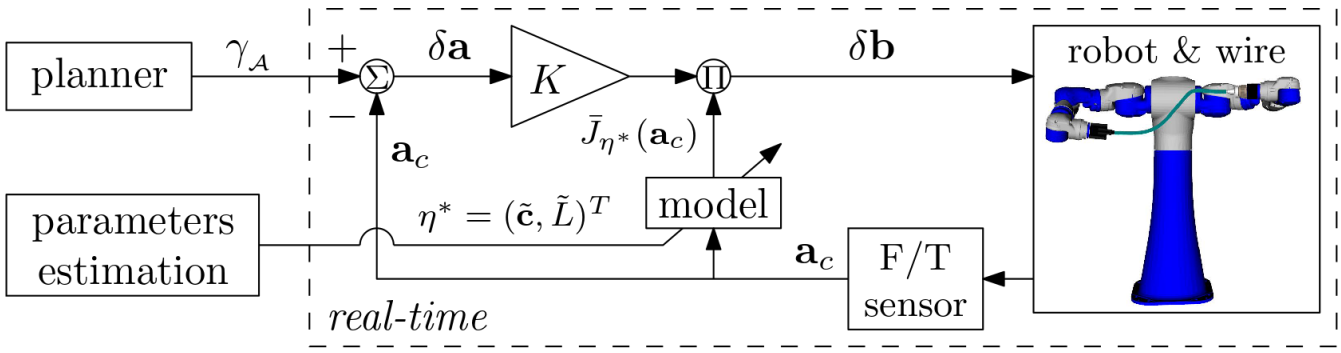

Fig. 2. Illustration of the control scheme. In an off-line operation, parameters estimation will estimate $\mathbf{c}$ and L, and update the model. Also, in an offline process, a planner plans a path to some goal. In the online process and given a goal configuration $\mathbf{a}_g$ or a path $\gamma_{\mathcal{A}}$ to track, the controller will provide the required perturbations of the second gripper. Feedback is acquired using a force/torque sensor on the base arm whom provides information about the current configuration $\mathbf{a}_c$ of the wire.

best local and global cost, and are aimed to both explore new regions and exploit local information. Since our goal is to estimate $\boldsymbol{\eta}$ in real-time, convergence to the best solution given some amount of data must be fast. Thus, a small population size is used. The particles are continuously updated when new measurements are acquired to refine $\boldsymbol{\eta}^*$. Moreover, to avoid convergence to local minima, we randomly sample new particles over the search space.

C. Control in $\mathcal{A}_{free}$

Given a wire goal configuration $(\mathbf{q}, \mathbf{u})_g \in \mathcal{C}$, directly controlling the path of the wire in $\mathcal{C}$ requires continuous visual feedback of its shape while the policy for moving the arms is not clear [9]. Alternatively, we propose to control the motion in $\mathcal{A}$ with no visual perception and based solely on F/T measurements. Given the current start configuration of the wire $\mathbf{a}_s \in \mathcal{A}_{free}$ and goal destination $\mathbf{a}_g \in \mathcal{A}_{free}$, we aim for a control rule for the grippers to manipulate the wire from $\mathbf{a}_s$ to $\mathbf{a}_g$. From perturbation mapping (11), we can formulate an iterative correction rule for the second gripper pose relative to the base as

$$\delta\mathbf{b}_i = K\bar{\mathbf{J}}_{\eta^*}(\tilde{\mathbf{a}}_i)(\mathbf{a}_g - \tilde{\mathbf{a}}_i) \tag{13}$$

where $\tilde{\mathbf{a}}_0 = \mathbf{a}_s$. The control gain $K > 0$ is chosen to constrain motion of the wire to small steps in order to enable frequent corrections of deviations. In addition, a small value for K prevents fast manipulations that could hinder the quasi-static motion required to maintain static equilibrium. According to (10), applying perturbation $\delta\mathbf{b}_i$ to the current configuration $\mathbf{b}_i$ of the second gripper (relative to the base gripper) yields

$$\mathbf{b}_{i+1} = \mathbf{b}_i M(\delta\mathbf{b}_i). \tag{14}$$

The value for $\tilde{\mathbf{a}}_{i+1}$ is acquired once the second gripper is moved to $\mathbf{b}_{i+1}$. The process is repeated for $i = 0, 1, \ldots, k$ until satisfying $\|\mathbf{a}_g - \tilde{\mathbf{a}}_i\| < \epsilon$ where $\epsilon > 0$ is an accuracy distance threshold in $\mathcal{A}$.

When no uncertainties exist, the motion will be on a straight line $\bar{\mathbf{a}}(\sigma) = \sigma(\mathbf{a}_g - \mathbf{a}_s) + \mathbf{a}_s$ for $\sigma \in [0, 1]$. If $\mathbf{a}_s$ and $\mathbf{a}_g$ are $\mathcal{A}$-connected [14], i.e., $\bar{\mathbf{a}}(\sigma) \in \mathcal{A}_{free}$ is satisfied for all $\sigma \in [0, 1]$, motion to $\mathbf{a}_g$ along $\bar{\mathbf{a}}(\sigma)$ is feasible. However, controller (13)-(14) ignores the kinematics of the dual-arm system and does not guarantee it can provide the required motion. Hence, tracking a planned path where these are constrained is presented next.

D. Path tracking

Let $\mathcal{Q}$ be the configuration space of the dual-arm system formed by their joint space product. The configuration space of the wire and robot system is defined as $\mathcal{Z} = \mathcal{A} \times \mathcal{Q}$. Furthermore, let $\mathcal{Z}_{free} \subset \mathcal{Z}$ be the set of configurations that satisfy joint limits, wire stability and collision-free. A motion planner, such as the one proposed in [16], would output a continuous path $\gamma : [0, 1] \to \mathcal{Z}_{free}$ from the current start configuration $\gamma(0) = (\mathbf{a}_s, \phi_s) \in \mathcal{Z}_{free}$ to a desired one $\gamma(1) = (\mathbf{a}_g, \phi_g) \in \mathcal{Z}_{free}$. Path $\gamma(s)$ with $s \in [0, 1]$ can be divided into $\gamma_{\mathcal{A}}(s) \in \mathcal{A}$ and $\gamma_{\mathcal{Q}}(s) \in \mathcal{Q}$. Planning in $\mathcal{Z}_{free}$ ensures that the path is feasible in terms of wire stability, obstacles and kinematics of the arms.

While the planning of path γ considers motion both in $\mathcal{Q}$ and $\mathcal{A}$, the tracking accuracy of the wire is prioritized for successful task completion. In open-loop control, however, tracking would be conducted by solely moving the arms along path $\gamma_{\mathcal{Q}}$ without the ability to reason about accuracy along $\gamma_{\mathcal{A}}$. Therefore, positioning inaccuracies and uncertainties may deviate the wire from the desired path $\gamma_{\mathcal{A}}$ in $\mathcal{A}_{free}$. Correcting deviations along $\gamma_{\mathcal{A}}$ is not possible in such approach. Alternatively, we propose to ignore $\gamma_{\mathcal{Q}}$ and control the motion to solely track $\gamma_{\mathcal{A}}$ using (13)-(14). Tracking would be performed on a set of N discrete points $\{\bar{\mathbf{a}}_0, \bar{\mathbf{a}}_1, \ldots, \bar{\mathbf{a}}_N\} \in \gamma_{\mathcal{A}}(s)$ where $\bar{\mathbf{a}}_i = \gamma_{\mathcal{A}}(\frac{i}{N})$. The path in $\mathcal{A}_{free}$ is now piece-wise linear and motion between each two points is controlled as described in Section III-C. While we ignore the planned path $\gamma_{\mathcal{Q}}$, if the model of the wire is sufficiently accurate, the true path $\tilde{\gamma}_{\mathcal{Q}}$ of the dual-arm system with (13)-(14) is expected to be approximately similar such that $\tilde{\gamma}_{\mathcal{Q}}(s) \approx \gamma_{\mathcal{Q}}(s)$.

IV. Experiments

To validate our approach and analyze performance, we have built an experimental setup comprised of the Yaskawa Motoman SDA10F dual-arm robot seen in Figure 1. On its left hand, we have mounted a six-axis F/T sensor (Bota SensONE). The F/T sensor has a gravity compensation module.

In addition, chuck grippers were fixed in both hands to hold the wires. A set of $V = 11$ fiducial markers was placed along the installed wire so that a motion capture system is able to provide ground-truth measurements of its shape in real-time. The system can be seen in Figure 1. All data acquisition, control and communication was implemented using the Robot Operating System (ROS) over an Ubuntu machine. Videos of the experiments and demonstration can be seen in the supplementary material.

A. Force/Torque sensor Calibration

Direct measurements of the F/T sensor do not reflect the pure force and torque that are exerted by the wire due to gripper fabrication uncertainties and intrinsic non-linearity of the sensor. Hence, we employ a machine learning based calibration process of the F/T sensor. We use a Nitinol wire with known length and mechanical coefficient vector $\mathbf{c}$ to collect labeled data. The wire is manipulated through various configurations while recording for each the F/T measurement $\bar{\mathbf{a}}_j$ and the corresponding set of marker locations $\mathcal{P}_j = \{\mathbf{p}_{j,1}, \dots, \mathbf{p}_{j,V}\}$ where $\mathbf{p}_{j,k} \in \mathbb{R}^3$ is the spatial position of marker k relative to the base gripper. For each sample $\{\bar{\mathbf{a}}_j, \mathcal{P}_j\}$, we compute the theoretical wire configuration $\mathbf{a}_j$ by solving the following minimization problem

$$\mathbf{a}_j = arg\min_{\mathbf{a}} \quad \sum_{k=1}^{V} \|\mathbf{p}_{j,k} - \mathbf{x}_k(\mathbf{a})\|^2 \tag{15}$$

where $\mathbf{x}_k \in \mathbb{R}^3$ is the closest point to $\mathbf{p}_{j,k}$ on a wire $(\mathbf{q}, \mathbf{u}) = \Phi(\mathbf{a})$. Problem (15) is solved off-line for each sample using PSO. Note that the solution of (15) is the inverse of Γ where the respected $\mathbf{a}$ is found based on a desired shape of the wire. The final product is a dataset comprised of K input samples $\{\bar{\mathbf{a}}_1, \dots, \bar{\mathbf{a}}_K\}$ and output labels $\{\mathbf{a}_1, \dots, \mathbf{a}_K\}$. The data is then used to train an Artificial Neural-Network (ANN) to map a perceived F/T measurement to the respected model-based configuration $\mathbf{a}$ of the wire. This process is done once. Then, the trained ANN can be deployed to acquire wire configurations in real-time and approximate $\mathbf{c}$ as described next.

B. Approximation of $\mathbf{c}$ and L

We have conducted an approximation of two Nitinol wires of 2 mm and 3 mm diameter with known mechanical coefficients.The second gripper was randomly moved while adding poses to $\mathcal{B}_c$ and F/T measurements to $\mathcal{A}_c$. The sampling frequency is 10 Hz. Using PSO with 20 particles, vector $\boldsymbol{\eta}$ was approximated by solving (12) while collecting data in real-time. Table I presents the average of the approximated values and their relative error after 10 repeated trials and for only three sampled points in $\{\mathcal{A}_c, \mathcal{B}_c\}$. Figure 3 presents the approximated values for the 3 mm diameter wire with regards to the number of recorded data points in $\{\mathcal{A}_c, \mathcal{B}_c\}$. The results show that with only two samples, the approximation accuracy is high. Adding more data points does not provide significant accuracy improvement. In addition, Figure 4 reports the convergence time to reach a solution given a number of samples.

TABLE I
ACCURACY RESULTS FOR MECHANICAL COEFFICIENTS AND LENGTH ESTIMATION OF A NITINOL WIRE

Diameter	Coefficient	True	Estimated	Relative Error (%)
2 mm	$\mathbf{c}_1$ (Nm^2)	0.042	0.043 $\pm$ 0.006	2.4
	$\mathbf{c}_2$ (Nm^2)	0.055	0.056 $\pm$ 0.008	1.8
	$\mathbf{c}_3$ (Nm^2)	0.055	0.056 $\pm$ 0.008	1.8
	L (m)	0.630	0.635 $\pm$ 0.012	0.8
3 mm	$\mathbf{c}_1$ (Nm^2)	0.214	0.215 $\pm$ 0.008	0.5
	$\mathbf{c}_2$ (Nm^2)	0.278	0.279 $\pm$ 0.011	0.4
	$\mathbf{c}_3$ (Nm^2)	0.278	0.279 $\pm$ 0.011	0.4
	L (m)	0.820	0.811 $\pm$ 0.013	1.1

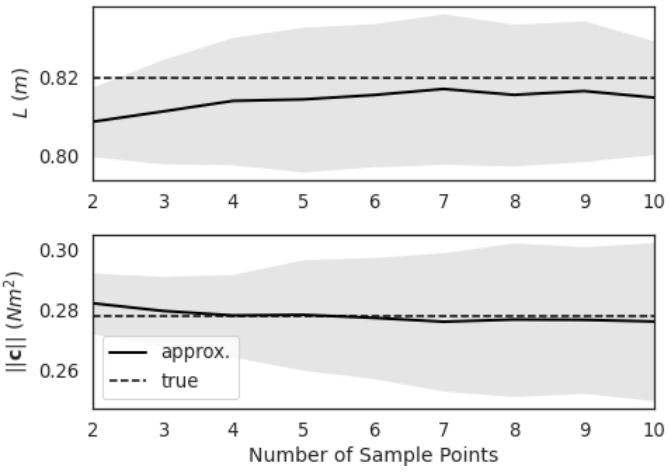

Fig. 3. Mean error and standard deviation for approximating $\mathbf{c}$ and L for the 3 mm diameter wire with regards to the number of sample points.

The results show that an accurate real-time approximation is available after only three seconds of motion while sensing only F/T and second gripper poses.

C. Wire shape estimation

In this section, we analyze the accuracy of shape estimation using the F/T measurements. Four wires are tested including three Nitinol wires of different lengths and diameters, and an electric cable made of copper with a polymeric insulator. For each wire, the mechanical properties were estimated. Then, pose estimation was averaged for 50 configurations in $\mathcal{A}_{free}$. Table II presents the mean and standard deviation shape errors for the tested wires. The results show that Nitinol wires

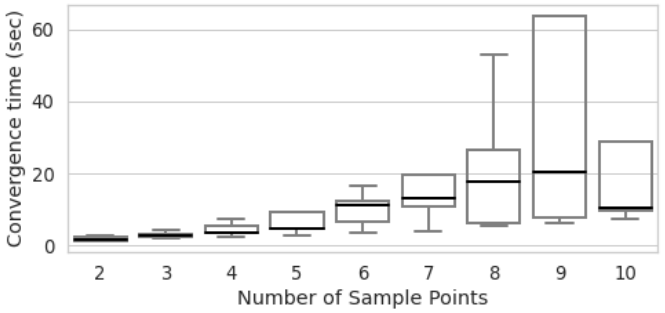

Fig. 4. Time to estimate $\mathbf{c}$ and L for the 3 mm diameter wire with regards to the number of samples taken.

TABLE II
ACCURACY RESULTS FOR SHAPE ESTIMATION OF VARIOUS WIRES

Num.	Wire type	Diameter (mm)	length (mm)	Mean Error (mm)
1	Nitinol	2	630	5.72 ± 2.58
2	Nitinol	3	910	7.42 ± 1.33
3	Nitinol	3	820	6.55 ± 0.87
4	Electric	3	920	52.3 ± 11.5

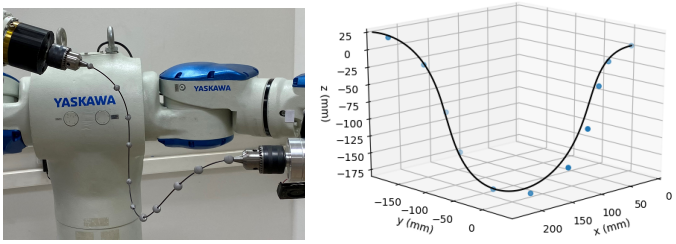

Fig. 5. Shape estimation of a wire configuration using only F/T measurement. The circular blue markers are the ground-truth measured using a motion capture system and the solid curve is the estimation. Average shape estimation error along the wire is 5.81 mm.

acquire high shape estimation accuracy since their mechanical properties comply with the assumption described in Section II-A. On the other hand, the electric wire is not straight in the relaxed form and highly affected by gravitation which is not included in the model. Hence, the electric cable does not comply with the assumptions of the model and large errors are exhibited. Figure 5 shows an example of one pose estimation with Nitinol wire number 3.

D. Control

In the first control experiment, we test the accuracy when manipulating the wire to given goals using (13). Hence, we sample 30 random start and goal configurations in $\mathcal{A}_{free}$ which are known to be $\mathcal{A}$-connected. Once the system is at a start configuration, the controller is applied to reach the corresponding goal. The controller gain was set to $K = 0.2$. We compare the control to an open-loop setting in which a straight line path from $\mathbf{a}_s$ to $\mathbf{a}_g$ is computed along with the corresponding gripper poses. Then, the gripper poses are rolled-out without any feedback. Furthermore, we test the performance in a case where the positioning of the grippers is inaccurate. Thus, we add random normal noise $\mathcal{N}(0, 10)\ mm$ and $\mathcal{N}(0, 3^\circ)$ to the position and orientation, respectively, of the control output $\delta\mathbf{b}_i$ in (13). Hence, we add inaccuracies to the relative pose between the two grippers.

Table III presents results of the mean shape error along the wire for open and closed loop control with and without adding noise. Without noise, the high accuracy of the robotic arms provides low errors in open-loop. However, inaccuracy of the arms (with noise) leads to poor goal reach. On the other hand, the proposed closed-loop control over $\mathcal{A}$ shows the ability to compensate these inaccuracies and maintain accuracy with and without noise. Figure 6 shows an example of motion towards a goal in the $\mathcal{A}$ in open and closed-loop control. Closed-loop control exhibits smoother motion along a straight line and better accuracy at the final configuration. Figure 7 shows

TABLE III
MEAN ACCURACY FOR REACHING GOALS

	Open-loop (mm)	Closed-loop (mm)
without noise	4.80 ± 1.19	9.67 ± 3.02
with noise	17.35 ± 9.54	9.11 ± 3.62

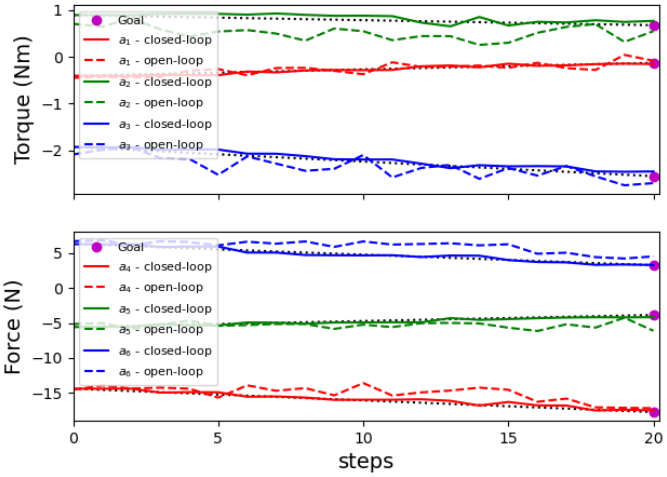

Fig. 6. Wire manipulation towards the goal in the $\mathcal{A}$ with open (dashed) and closed-loop (solid) control. Dotted lines illustrate the nominal straight line path in $\mathcal{A}$.

the corresponding wire shape errors in $\mathcal{C}$ relative to the shape $(\mathbf{q}, \mathbf{u})_g = \Phi(\mathbf{a}_g)$. The figure also shows (in dotted lines) the error for moving along a straight line in $\mathcal{B}$ without considering F/T measurements. Closed-loop control clearly reaches closer to the desired shape. It is important to note that, while the control converges to the desired configuration in $\mathcal{A}$, the error in $\mathcal{C}$ did not converge to zero due to inaccuracies of the F/T sensor calibration model described in Section IV-A. Overall, the results exhibit good accuracy in reaching various goals with control regardless of arm inaccuracies.

We now experiment the tracking of a path with open and closed loop control as discussed in Section III-D while including the same noise. We have implemented the asymptotically optimal variant of the Rapidly-exploring Random Tree, i.e., RRT* [24]. The RRT* planner ensures that the path from $\mathbf{a}_s$ to $\mathbf{a}_g$ is in $\mathcal{A}_{free}$ while minimizing path length. For a set of ten arbitrary start and goal configurations, we have planned and rolled-out the paths in open and closed loop control. Table IV presents the mean and maximum shape error along the paths. Furthermore, Figures 8 and 9 show

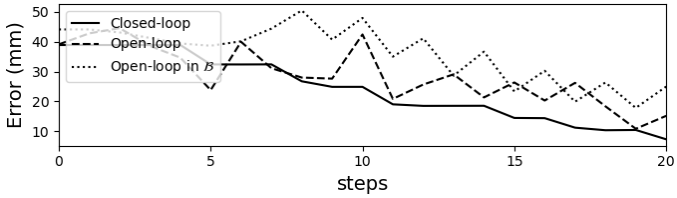

Fig. 7. Wire shape error during manipulation to the goal $\mathbf{a}_g$ with open (dashed) and closed-loop (solid) control. Dotted curve show the error for an open-loop while tracking a straight line path in $\mathcal{B}$.

TABLE IV
ACCURACY OF PATH TRACKING

	Open-loop (mm)	Closed-loop (mm)
Mean	11.01 ± 5.21	6.22 ± 1.83
Max.	31.51	11.62

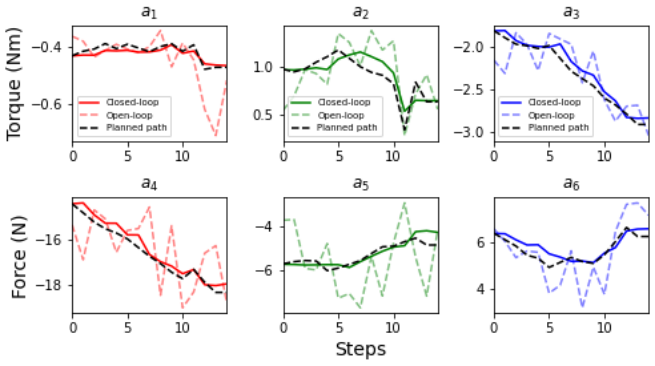

Fig. 8. Tracking of a path in $\mathcal{A}$ planned using RRT* with open (dashed) and closed-loop (solid) control. Black dashed lines illustrate the planned path to track in $\mathcal{A}$.

an example of tracking one path. The fine tracking along the planned path with closed-loop control is shown compared to non-smooth and erroneous tracking with open-loop. Snapshots of the motion with pose estimation are shown in Figure 10. Here also, the small tracking errors in closed-loop are imposed by accuracy of the F/T sensor calibration. Nevertheless, these experiments validate the ability of the proposed closed-loop control to maintain good tracking along planned paths.

E. Demonstration

We have conducted a demonstration in which the robot must manipulate the wire through a narrow passage formed by two obstacles. The width of the narrow passage is 50 mm. Two start and goal configurations were chosen and a path between them was planned using RRT*. Then, the path was rolled-out with open and closed-loop control in real-time for ten attempts each. Here also, normal noise was included similar to previous sub-section. Failure is declared when the wire collides with an obstacle and can be detected when large deviations in the F/T measurements occur in a short period of time. Figures 11-12 show the path tracking of roll-outs in open-loop with a collision and closed-loop control. Once the wire has collided, the F/T measurements include contact

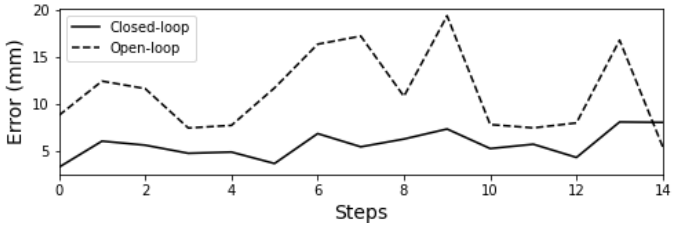

Fig. 9. Average shape error of the wire during path tracking with open and closed-loop control.

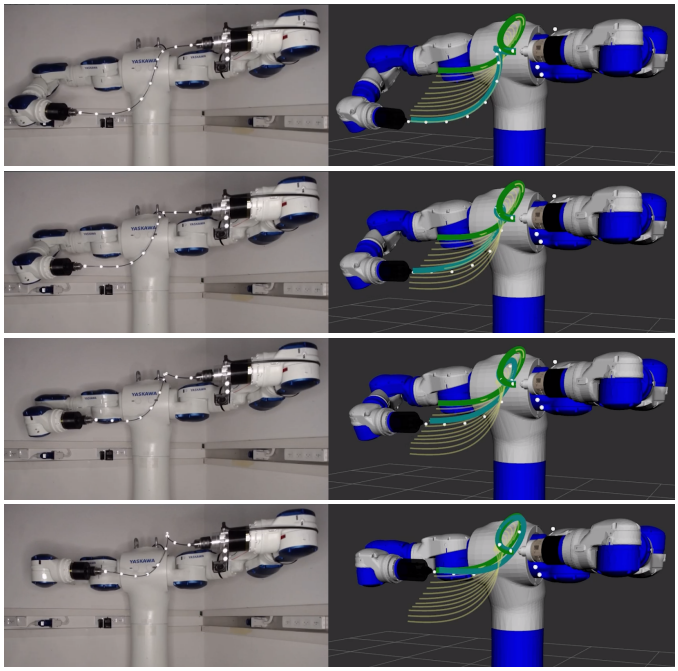

Fig. 10. The wire is controlled to track a path in $\mathcal{A}_{free}$ planned with RRT*. White circles are the measured markers along the wire and the cyan curve shows the current pose estimation based on F/T sensing. Yellow curves indicate intermediate configurations to pass along the motion while the green curve illustrates the goal. Mean shape error across the manipulation is $6.2mm$.

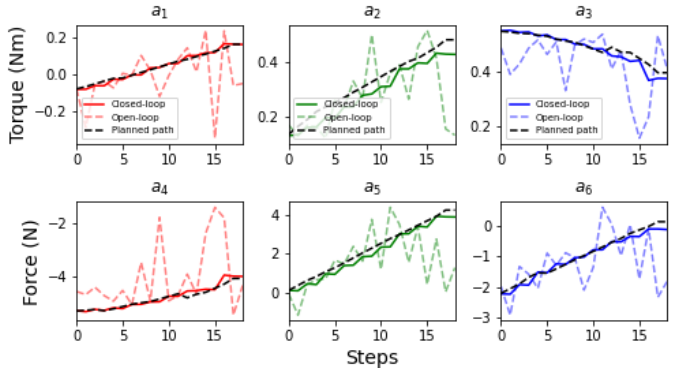

Fig. 11. Roll-out of the path between the obstacles in open (dashed) and closed-loop (solid) control. Black dashed lines illustrate the planned path to track in $\mathcal{A}$. The roll-out in open-loop collided and the F/T measurements significantly deviated from the planned path in $\mathcal{A}$.

loads and it is no longer possible to estimate the shape of the wire in order to return to the path. Due to better tracking with control, the success rates for tracking the path with open- and closed-loop control are 30% and 90%, respectively. Figure 13 shows snapshot of one successful roll-out with closed-loop control. The demonstration results validate the accurate tracking and emphasize the importance of accurate path tracking in cluttered environments.

V. CONCLUSIONS

We have addressed the problem of estimating the shape of a wire solely based on F/T measurements at the base gripper. A complete framework has been proposed where the mechanical properties of the wire are rapidly approximated and the wire can be accurately manipulated with closed-loop control. The shape of the wire is controlled in the configuration space of the

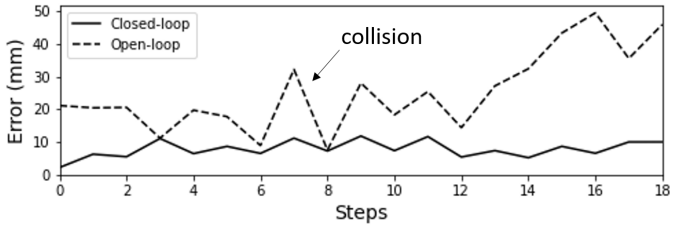

Fig. 12. Average shape error of the wire during path tracking between the obstacles with open and closed-loop control. The roll-out in open-loop collided and the motion significantly deviated from the planned path.

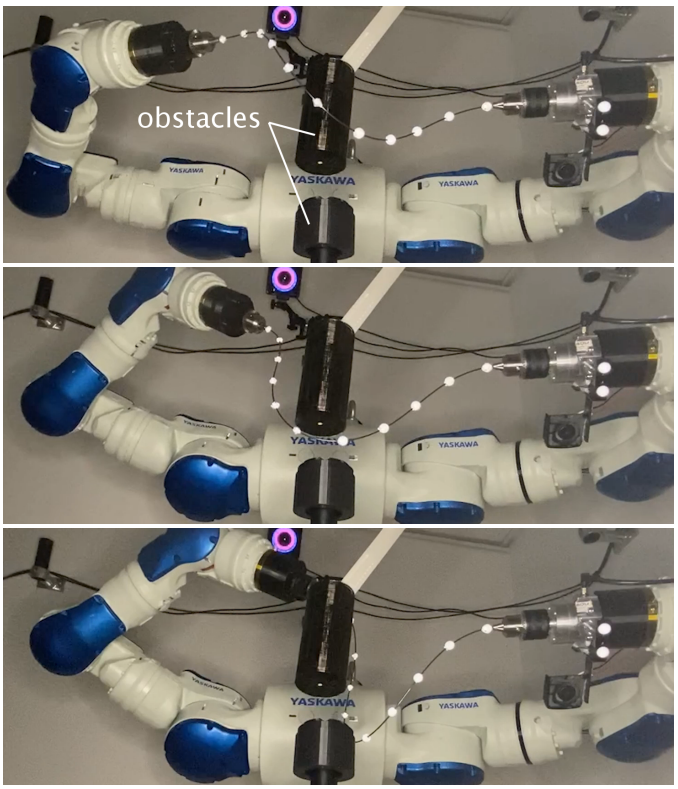

Fig. 13. Snapshots of the robot manipulating the wire between obstacles in closed-loop control with F/T feedback.

wire rather then in space of gripper poses. In such way, the manipulation can be performed without explicit information on the spatial shape of the wire. The experiments have shown that, indeed, accurate manipulations can be performed without complex visual perception. We have also evaluated the control of the wire in $\mathcal{A}$. Open-loop control has been shown to be feasible when the robotic arms are accurate. Nevertheless, closed-loop control maintains accurate manipulations even when the accuracy of the arms is low. Future work may combine visual perception and F/T measurement to reduce estimation inaccuracies. Additionally, an algorithmic solution is required in order to detect the location of collisions in order to retract properly. Machine learning methods could be incorporated into the model in order to reduce the effects of obstacle disturbances and uncertainties when manipulating wires, such as the electric cable, that do not comply with the model assumptions.

REFERENCES

[1] R. Levien, "The elastica: a mathematical history," EECS Department, University of California, Berkeley, Tech. Rep., Aug 2008.
[2] K. Kosuge, H. Yoshida, T. Fukuda, M. Sakai, and K. Kanitani, "Manipulation of a flexible object by dual manipulators," in *Proc. IEEE Int. Conf. on Rob. and Aut.*, vol. 1, 1995.
[3] M. Takizawa, S. Kudoh, and T. Suehiro, "Implementation of twisting skill to robot hands for manipulating linear deformable objects," in *IEEE/RSJ International Conference on Intelligent Robots and Systems (IROS)*, 2016, pp. 945–950.
[4] X. Jiang, K.-M. Koo, K. Kikuchi, A. Konno, and M. Uchiyama, "Robotized assembly of a wire harness in a car production line," *Advanced Robotics*, vol. 25, no. 3-4, pp. 473–489, 2011.
[5] J. Schulman, J. Ho, C. Lee, and P. Abbeel, *Learning from Demonstrations Through the Use of Non-rigid Registration*, 2016, pp. 339–354.
[6] R. C. Jackson and M. C. Çavuşoğlu, "Needle path planning for autonomous robotic surgical suturing," in *Proc. IEEE Int. Conf. on Rob. and Aut.*, 2013, pp. 1669–1675.
[7] S. Duenser, R. Poranne, B. Thomaszewski, and S. Coros, "Robocut: Hot-wire cutting with robot-controlled flexible rods," *ACM Transactions on Graphics*, vol. 39, no. 4, 2020.
[8] F. Augugliaro, E. Zarfati, A. Mirjan, and R. D'Andrea, "Knot-tying with flying machines for aerial construction," in *IEEE/RSJ Inter. Conference on Intelligent Robots and Systems*, 2015, pp. 5917–5922.
[9] F. Lamiraux and L. E. Kavraki, "Planning paths for elastic objects under manipulation constraints," *International Journal of Robotics Research*, vol. 20, pp. 188–208, 2001.
[10] M. Moll and L. E. Kavraki, "Path planning for deformable linear objects," *IEEE Trans. on Robotics*, vol. 22, no. 4, pp. 625–636, 2006.
[11] T. Hermansson, R. Bohlin, J. S. Carlson, and R. Söderberg, "Automatic assembly path planning for wiring harness installations," *Journal of Manufacturing Systems*, vol. 32, no. 3, pp. 417 – 422, 2013.
[12] I. Kabul, R. Gayle, and M. C. Lin, "Cable route planning in complex environments using constrained sampling," in *Proc. of the ACM Symposium on Solid and Physical Modeling*, NY, 2007, pp. 395–402.
[13] R. Gayle, P. Segars, M. Lin, and D. Manocha, *Path planning for deformable robots in complex environments*. MIT Press Journals, 2005, vol. 1, pp. 225–232.
[14] T. Bretl and Z. Mccarthy, "Quasi-static manipulation of a kirchhoff elastic rod based on a geometric analysis of equilibrium configurations," *Int. Jou. of Robotics Research*, vol. 33, no. 1, pp. 48–68, 2014.
[15] O. Roussel, A. Borum, M. Taïx, and T. Bretl, "Manipulation planning with contacts for an extensible elastic rod by sampling on the submanifold of static equilibrium configurations," in *Proc. IEEE Int. Conf. on Rob. and Aut.*, 2015, pp. 3116–3121.
[16] A. Sintov, S. Macenski, A. Borum, and T. Bretl, "Motion planning for dual-arm manipulation of elastic rods," *IEEE Robotics and Automation Letters*, vol. 5, no. 4, pp. 6065–6072, 2020.
[17] A. Borum, D. Matthews, and T. Bretl, "State estimation and tracking of deforming planar elastic rods," in *IEEE International Conference on Robotics and Automation*, Sep. 2014, pp. 4127–4132.
[18] N. Nakagawa and H. Mochiyama, "Real-time shape estimation of an elastic rod using a robot manipulator equipped with a sense of force," in *IEEE/RSJ International Conference on Intelligent Robots and Systems*, 2018, pp. 8067–8073.
[19] S. Javdani, S. Tandon, J. Tang, J. F. O'Brien, and P. Abbeel, "Modeling and perception of deformable one-dimensional objects," in *IEEE Inter. Conf. on Robotics and Automation*, 2011, pp. 1607–1614.
[20] J. Zhu, B. Navarro, P. Fraisse, A. Crosnier, and A. Cherubini, "Dual-arm robotic manipulation of flexible cables," in *IEEE/RSJ Inter. Conference on Intelligent Robots and Systems*, 2018, pp. 479–484.
[21] R. Takano, H. Mochiyama, and N. Takesue, "Real-time shape estimation of kirchhoff elastic rod based on force/torque sensor," in *IEEE Inter. Conf. on Robotics and Automation (ICRA)*, 2017, pp. 2508–2515.
[22] S. Antman, *Nonlinear Problems of Elasticity*. Springer, 2005.
[23] J. Kennedy and R. Eberhart, "Particle swarm optimization," in *International Conference on Neural Networks*, vol. 4, 1995, pp. 1942–1948.
[24] S. Karaman and E. Frazzoli, "Sampling-based algorithms for optimal motion planning," *International Journal of Robotics Research*, vol. 30, no. 7, pp. 846–894, Jun. 2011.